JOURNAL OF MATERIALS SCIENCE: MATERIALS IN MEDICINE 6 (1995) 138–143

Mechanical properties of hydroxyapatite formed at physiological temperature

R. I. MARTIN, P. W. BROWN
Department of Materials Science and Engineering, The Pennsylvania State University, University Park PA 16802, USA

The mechanical properties of monoliths of calcium-deficient and carbonated hydroxyapatite formed by dissolution–precipitation reactions at 38 °C have been determined. Particulate solid reactants were mixed at liquid-to-solid weight ratios of 0.11 and 0.2 and pressed into various configurations on which mechanical tests were carried out. Testing was performed on wet specimens which had been allowed to react for 8 h by which time phase-pure hydroxyapatite had formed. Calcium-deficient hydroxyapatite produced at a liquid-to-solids ratio of 0.11 exhibited a tensile strength as high as 18 MPa, an average compressive strength of 174 MPa and a Young's modulus of 6 GPa. These values were lower when a larger proportion of water (liquid-to-solid 0.2) was used in sample preparation. However, the compressive strengths of calcium-deficient hydroxyapatite prepared at 38 °C are comparable to the compressive strengths of sintered hydroxyapatite containing an equivalent total porosity. Carbonated hydroxyapatite showed mechanical properties inferior to those exhibited by calcium-deficient material. These differences appear to be related to the microstructural variations between these compositions.

1. Introduction

The mechanical properties of sintered hydroxyapatite have been well characterized. As a structural material hydroxyapatite is a very brittle ceramic which is strong in compression and weak in tension. Compressive strengths as high as 917 MPa have been reported [1]. By way of comparison, compressive strength values reported for enamel and dentin have been reported as 384 and 295 MPa, respectively [2].

A linear dependence of both Young's modulus and Poisson's ratio on the density of sintered hydroxyapatite were found over the range of densities from 75% of theoretical and upwards [5]. A logarithmic decrease of compressive strength with porosity over the range from about 8 vol % to about 70 vol % has been demonstrated [6].

Values for the fracture toughness of enamel range from about 0.7 to 1.3 MPa $m^{1/2}$ [7]. de With *et al.* [5] reported the fracture toughness of sintered hydroxyapatite to reach values as high as $K_{Ic} = 1$ MPa $m^{1/2}$ as the porosity was reduced to 5%. Flexural strengths of 115 MPa were observed on similar materials. Higher flexural strengths, approaching 150 MPa, were observed in mixed HAp–TCP ceramics [8]. Mechanical properties of sintered synthetic hydroxyapatite depending on the sintering temperature have been reported by Aoki [9] and are listed in Table I.

The porosities achieved varied with the sintering temperature. The porosities of hydroxyapatite sintered at 1150 °C and 1300 °C were approximately 20 vol % and 4 vol %, respectively. These values also fall on the curve reported by Williams [6] relating compressive strength to volume porosity. Aoki [9] found transgranular fracture occurs below 4 vol % and intergranular fracture occurs above 9 vol % in sintered hydroxyapatite. Recently it has become possible to produce phase-pure hydroxyapatite by chemical reaction at low temperature [10, 11]. Low temperature formation has typically resulted in hydroxyapatite monoliths which exhibit relatively poor mechanical properties. For example, the compressive strength of hydroxyapatite containing approximately 50% porosity is 31 MPa [10]. Other values of compressive strengths reported are in the range 34–51 MPa [12–14].

The mechanical properties of hydroxyapatite monoliths produced at low temperature are of particular interest because monoliths formed in this way may also be formed *in vivo*. As a consequence a variety of prosthetic applications in dentistry and orthopaedics may be realized. However, such applications would benefit from the preparation of hydroxyapatite which exhibits improved mechanical properties. This paper explores the mechanical properties of wet apatite monoliths that are formed in aqueous solutions at physiological temperature.

2. Experimental procedure

Calcium-deficient HAp and carbonated HAp can be formed at low temperature by the following two reac-

0957–4530 © *1995 Chapman & Hall*

TABLE I Compressive and flexural properties of sintered hydroxyapatite [9]

Temperature (°C)	Compressive strength σ_C (MPa)	Flexural strength σ_C (MPa)	Modulus of elasticity in compression E_C (GPa)	Modulus of elasticity in bending E_B (GPa)
1150	308 ± 46	61 ± 8	42.2 ± 3.8	44.3 ± 3.5
1200	415 ± 46	104 ± 11	74.6 ± 4.1	80.0 ± 6.4
1250	465 ± 58	106 ± 10	79.0 ± 4.8	85.1 ± 6.1
1300	509 ± 57	113 ± 12	81.4 ± 4.6	87.8 ± 6.0

tions [15]:

$$6CaHPO_4 + 3Ca_4(PO_4)_2O \Rightarrow 2Ca_9HPO_4(PO_4)_5OH + H_2O \quad (1)$$

$$\tfrac{5}{8}NaHCO_3 + 2CaHPO_4 + 2Ca_4(PO_4)_2O \Rightarrow \times 1.067Ca_{9.375}Na_{0.586}(PO_4)_{5.375} \times (CO_3)_{0.586}(OH)_{1.961} + \tfrac{5}{16}H_2O \quad (2)$$

The precursors to $Ca_9HPO_4(PO_4)_5OH$ and carbonated hydroxyapatite were formed as monoliths. The precursors were mixed with water at 38 °C using liquid-to-solids weight ratios of 0.11 and 0.2, and pressed into bars at 38 °C and 70 MPa. Once the shapes of the monoliths were defined the specimens were removed from the moulds and placed immediately in a humid atmosphere at 38 °C. After curing for 8 h, the monoliths were tested for compressive strength and bending strength, and Young's modulus E was calculated. Samples were kept moist continuously. The diametral test and three-point bend test were used to determine tensile properties and compressive properties.

Deformation at the contact points is zero in the directions perpendicular to the loading direction. Discs of the two apatite compositions were made by pressing the precursors in a cylindrical die having a diameter of 1.27 cm at a compaction pressure of 70 MPa for 0.5 min. The discs were placed in storage vials with wet cotton balls to maintain high humidity and the vials were floated in a 38 °C water bath during HAp formation. The samples were left wet at 38 °C until they were tested. A model TTBML Instron was used to apply a diametral compressive force to the discoids at a constant rate of 0.01 cm/min and graphs of force versus time were obtained. A single sheet of paper towel was pressed into the top and the bottom of the specimen to compensate for any irregularities of the cylindrical surface in contact with the Instron's flat platens and thus promote a uniform distribution of applied load along the cylindrical axis.

A disc can physically represent a Mohr circle and the modes of failure can be observed. For failure in shear a wedge at 45° to the applied load with its tip pointing at the centre of the disc will split the remaining portion of the disc. For failure in tension a disc will simply split with its diametral plane parallel to the direction of the applied load and the cylindrical axis. The equation for calculating the ultimate tensile strength is:

$$\sigma_{ult} = \frac{2P}{\pi Dt} \quad (3)$$

where P is the applied load, D is the diameter and t is the thickness. Rudnick and coworkers [16] reported the factors that influence the test results and calculation.

Three-point bend tests were also performed by the same model TTBML Instron at a constant deformation rate of 0.01 cm/min with the lower reactionary supports spaced 9.53 mm apart. Typical dimensions of bend specimens are 3.18 cm long, 1 cm wide and 0.016 cm thickness. From the rectangular geometry, the maximum load P_m and the maximum deformation δ_m, the ultimate strength σ_{ult} and Young's modulus E can be computed according to the following equations [17]:

$$\sigma_{ult} = \frac{M_{max}c}{I} = \frac{P_m Lc}{4I} \quad (4)$$

$$E = \frac{P_m L^3}{48\delta_m I} \quad (5)$$

where the moment of inertia I is given by

$$I = \frac{bh^3}{12} \quad (6)$$

and P_m is the maximum load, L the span of the reactionary supports, c is one-half the height, and δ_m is the maximum deformation in the y direction.

A Tinius–Olsen universal testing machine was used to perform compressive tests on moist cylindrical apatite monoliths at a constant deformation rate of 0.01 cm/min. Compressive loading was applied in the z-axis direction.

3. Results and discussion

The formation of hydroxyapatite in aqueous solutions results in an apatite with a similar crystal structure, crystal defects and surface phenomena to bone mineral. Fig. 1 shows a comparison of the X-ray diffraction patterns of bone mineral and low-temperature hydroxyapatite at 38 °C, and both materials after heat treating at 700 °C for 16 h. It is apparent that bone mineral is best imitated by apatite formation involving an aqueous phase rather than by high-temperature, solid-state formation.

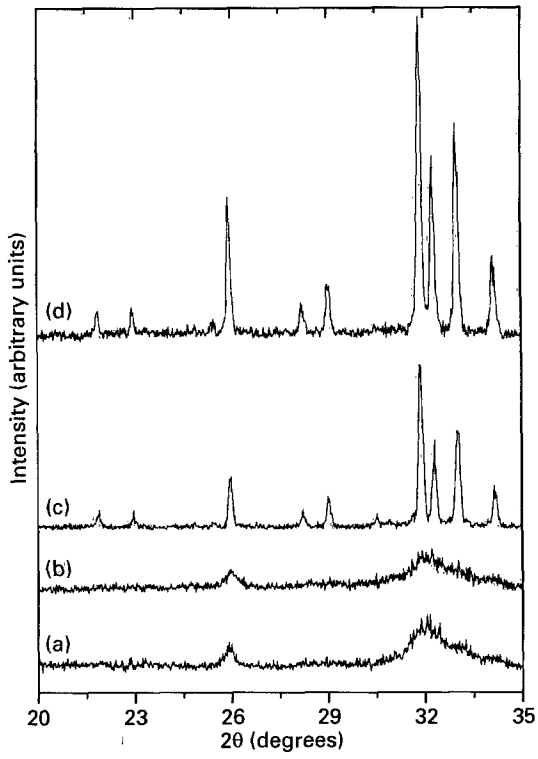

Figure 1 The powder X-ray diffraction patterns of bone mineral (a) and carbonated hydroxyapatite (b) formed at 38 °C, and after heat treatment for 16 h at 700 °C ((c), (d), respectively).

3.1. Tensile properties

Moist apatite monoliths were subjected to three different strength tests; diametral-compression test, three-point bend test and compression test. The mechanical properties are tabulated in Tables II–IV. The tensile and compressive properties show a dependence on both the liquid-to-solids ratio and the composition.

A typical stress–strain curve from the diametral-compression test and three-point bend test is a straight line. The brittle nature of hydroxyapatite is apparent by this linear stress–strain proportionality and abrupt failure. The average tensile strength is 13.1 MPa as determined from diametral compression of three samples of calcium-deficient hydroxyapatite formed at 38 °C and a liquid-to-solids ratio of 0.11. The slightly higher average of 15.2 MPa was obtained from the three-point bend tests of the same material

TABLE II Tensile properties obtained from disc samples with a constant strain rate applied perpendicular to the *z*-axis for a diametral-compression test

Type	L/S	Dia. (mm)	Thickness (mm)	σ_{ult} (MPa)
Cal.-def. HAp	0.11	12.61	1.451	13.3
Cal.-def. HAp	0.11	12.59	1.152	14.2
Cal.-def. HAp	0.11	12.60	1.089	11.8
Cal.-def. HAp	0.2	12.58	0.822	8.74
Cal.-def. HAp	0.2	12.62	0.991	7.36
Carbonated HAp	0.11	12.61	1.286	8.85
Carbonated HAp	0.11	12.61	1.266	11.9
Carbonated HAp	0.11	12.57	0.936	9.55
Carbonated HAp	0.2	12.60	1.553	8.13
Carbonated HAp	0.2	12.59	0.911	11.2

TABLE III Tensile properties obtained from a three-point bend test of rectangular bars with a constant strain rate applied

Type	L/S	Width (mm)	Height (mm)	σ_{ult} (MPa)	E (GPa)
Cal.-def. HAp	0.11	10.20	1.672	14.7	4.76
Cal.-def. HAp	0.11	10.22	1.678	18.3	5.14
Cal.-def. HAp	0.11	10.23	1.704	12.6	4.67
Cal.-def. HAp	0.2	10.22	1.607	15.4	6.04
Cal.-def. HAp	0.2	10.23	1.600	11.2	3.98
Cal.-def. HAp	0.2	10.20	1.530	12.9	3.99
Carbonated HAp	0.11	10.19	1.662	13.0	3.90
Carbonated HAp	0.11	10.21	1.634	–	–
Carbonated HAp	0.11	10.21	1.612	11.1	2.60
Carbonated HAp	0.2	10.18	1.570	14.2	2.45
Carbonated HAp	0.2	10.20	1.590	–	–
Carbonated HAp	0.2	10.15	1.592	9.40	2.23

TABLE IV Compression properties obtained from cylindrical samples with a constant strain rate applied parallel to the *z*-axis

Type	L/S	Dia. (mm)	Height (mm)	σ_{ult} (MPa)	E (GPa)
Cal.-def. HAp	0.11	6.41	6.39	–	–
Cal.-def. HAp	0.11	6.41	4.43	172	6.05
Cal.-def. HAp	0.11	6.42	5.09	173	7.31
Cal.-def. HAp	0.2	6.41	6.38	144	7.05
Cal.-def. HAp	0.2	6.42	6.15	129	6.94
Cal.-def. HAp	0.2	6.40	5.79	83.5	5.97
Carbonated HAp	0.11	6.38	6.20	75.0	5.59
Carbonated HAp	0.11	6.39	5.85	57.1	5.01
Carbonated HAp	0.11	6.39	6.38	59.4	4.87
Carbonated HAp	0.2	6.39	5.55	52.7	4.58
Carbonated HAp	0.2	6.41	5.45	75.5	5.23
Carbonated HAp	0.2	6.39	5.74	80.2	5.43

preparation. The major difference between the test methods is that diametral compression causes a sample to fail internally in a weak area on a plane in the volume unexposed to edge flaws, and three-point bending causes a sample to fail at a weak point on a line skewering potential critical flaws on the sample surface. It is possible the wet state of these samples reduces the effect of flaws on the mechanical behaviour of these apatite monoliths.

The carbonated hydroxyapatite monoliths show a similar trend in the mechanical properties. These are also listed in Tables II and III.

An increase in liquid-to-solids ratio from 0.11 to 0.2 reduced the average tensile strength 38% according to the diametral compression test and 13% according to the three-point bend test. The microporosity increases with increased liquid-to-solids ratio and the tensile strength decreases without significantly increasing critical surface flaws. Again, a similar trend is seen in the mechanical properties listed in Table II and Table III for carbonated hydroxyapatite.

3.2. Compressive properties

The compressive properties from direct compression of cylindrical samples in the *z* direction exhibit the greatest compositional dependence. Fig. 2 compares

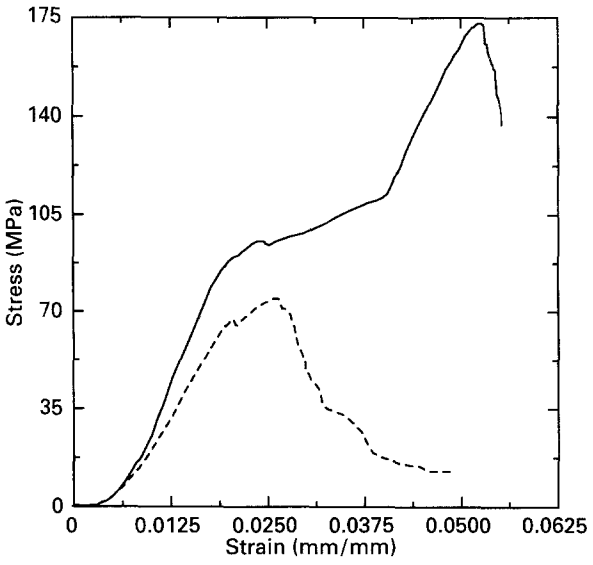

Figure 2 Typical stress–strain curves produced by applying a constant strain rate of 0.01 cm/min during compression tests of calcium-deficient hydroxyapatite (——) and carbonated hydroxyapatite (– – – –).

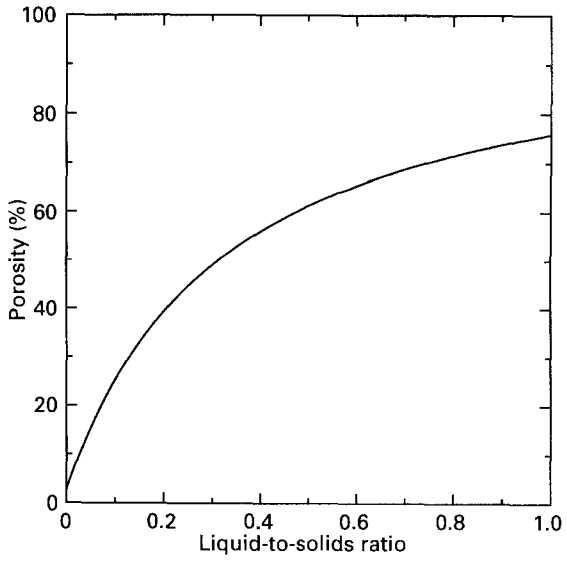

Figure 3 The relationship between the residual porosity and the liquid-to-solids ratio used during the low-temperature formation of hydroxyapatite.

the stress–strain curves from tests on wet cylinders of $Ca_9HPO_4(PO_4)_5OH$ and carbonated hydroxyapatite. $Ca_9HPO_4(PO_4)_5OH$ failed in a tensile mode while the carbonated hydroxyapatite failed in a shear mode. Calcium-deficient hydroxyapatite had numerous tensile plane failures occur between 90 MPa and 115 MPa and then, without further failure, the stress increased to approximately 170 MPa. The prisms that formed from the numerous tensile plane failures apparently were free of tensile flaws which allowed for higher strengths to be reached while the sum of the cross-sectional areas of the numerous prisms remained nearly equal to the original cross-sectional area of the cylinder. The final failure occurred abruptly as the prisms buckled in rapid succession. The effect of carbonation resulted in two cones with bases against the supports while radial pieces spawled off the cylindrical surface. Increasing the liquid-to-solids ratio reduced mechanical values but the stress–strain curves remained similar to those shown in Fig. 2. The values in Table IV show only a 31% strength reduction in $Ca_9HPO_4(PO_4)_5OH$ due to increasing the liquid-to-solids ratio from 0.11 to 0.2, while the effect of carbonation results in a 63% strength reduction. There was no noticeable reduction in the strength of carbonated hydroxyapatite by increased liquid-to-solids ratio.

3.3. The effect of porosity on compressive strengths

The final porosity in the monoliths depends on the liquid-to-solids ratio used at the beginning of the reaction in Equation 1. Fig. 3 shows the nonlinear dependence of porosity on the liquid-to-solids ratio R. Theoretically if the reaction in Equation 1 could be driven forward when R is equal to zero a lower limit of approximately 3 vol % porosity would result because of the reaction water produced. The curve in Fig. 3 is initially steep which indicates very low liquid-to-solids ratios must be used to achieve any significant mechanical integrity. The equation for this curve is

$$\text{vol \% porosity} = \frac{(C + 1)R + C}{(C + 1)R + c + 1/\rho_{HAp}} \times 100 \quad (7)$$

where R is the liquid-to-solids ratio, ρ is the density of hydroxyapatite and C is the weight ratio of reaction water and hydroxyapatite. C is 9.00×10^{-3} for Equation 1. The two values for R used in this investigation are 0.11 and 0.2 which correspond to 27 and 39 vol % porosity, respectively. These values for porosity and compressive strength of hydroxyapatite formed at low temperature agree with the logarithmic curve relating compressive strength to volume porosity reported for sintered hydroxyapatite by Williams [6]. Fig. 4 shows

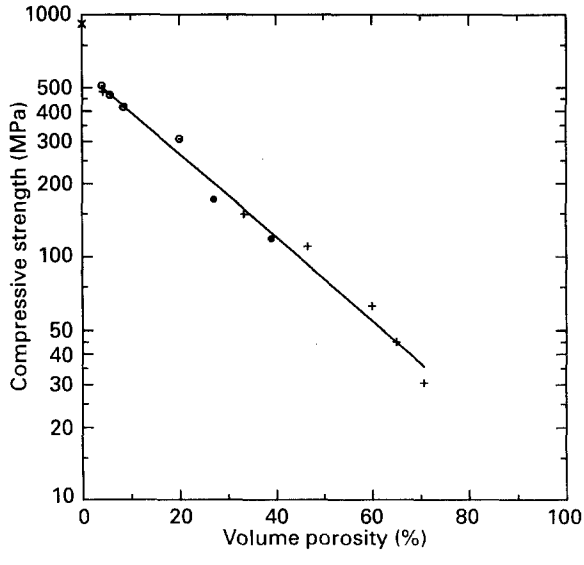

Figure 4 Ultimate strength of hydroxyapatite formed at high temperature and the reduction of strength with increased microporosity (× [1]; + [6]; ○ [9]; ● this study).

the logarithmic relationship between porosity and compressive strength as found by Williams and Aoki [6, 9]. The curve was calculated by applying the least-squares numerical method for a line to all the data points between 4 and 70 vol %. As Fig. 4 shows, the compressive strengths of the calcium-deficient hydroxyapatite prepared in this investigation fall on the curve. Thus, there is no reduction in compressive strength which occurs as a result of forming hydroxyapatite at low temperature.

3.4. Fracture surfaces and microstructure

The tensile fracture surfaces of calcium-deficient and carbonated hydroxyapatite monoliths were viewed by an Environmental scanning electron microscope (SEM) without the application of a conductive coating, and the microstructures of tensile fracture surfaces present after mechanical testing were observed. The micrograph in Fig. 5 shows the microporosity and crystallites of $Ca_9HPO_4(PO_4)_5OH$ formed at a liquid-to-solids ratio of 0.11 and 38 °C. There are two distinguishable morphologies; solid grains cemented together and needles of hydroxyapatite that form reticulated structures between the more solid grains. The same two morphologies are seen in Fig. 6 where

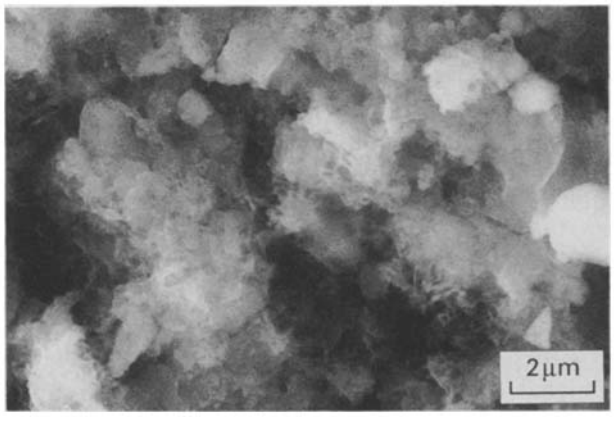

Figure 5 Tensile fracture surface of calcium-deficient hydroxyapatite formed at a liquid-to-solids ratio of 0.11 at 38 °C.

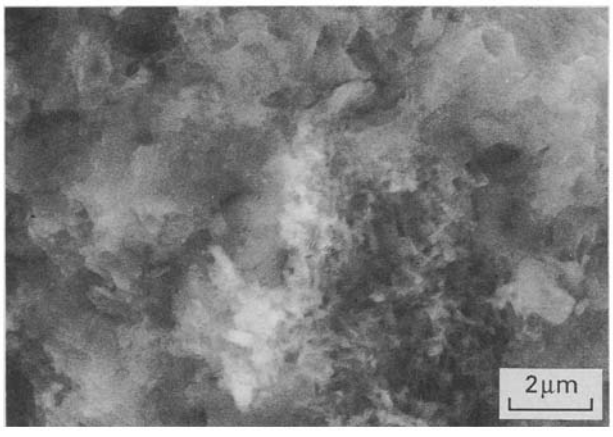

Figure 6 Tensile fracture surface of calcium-deficient hydroxyapatite formed at a liquid-to-solids ratio of 0.2 at 38 °C.

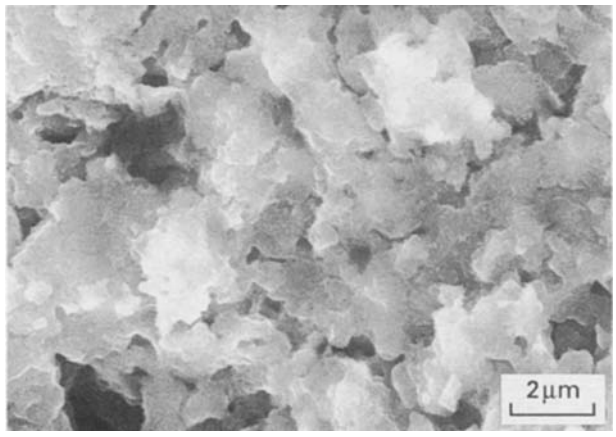

Figure 7 Tensile fracture surface of carbonated hydroxyapatite formed at a liquid-to-solids ratio of 0.11 at 38 °C.

the liquid-to-solids ratio was increased to 0.2. Compared to Fig. 5 slightly larger pores can be seen in Fig. 6.

Fig. 7 is a micrograph of fracture surfaces from the carbonated hydroxyapatite monoliths having the same processing history as the calcium-deficient hydroxyapatite monoliths. The difference is $NaHCO_3$ particles were mixed with the HAp precursors before hydration at 38 °C. The presence of carbonate has a definite effect on morphology. Only one of the two morphologies seen in Figs 5 and 6 can be seen in Fig. 7; cemented solid grains. There are no hydroxyapatite needles or reticulated networks observable. Larger pores can be seen in Fig. 7 than in Figs 5 and 6. Thus, the reduction in mechanical properties and the change in the mode of failure may be due to the lack of bridging HAp needles between the dense regions.

4. Summary

Moist monoliths of hydroxyapatites exhibit an elastic stress–strain relationship. Calcium-deficient hydroxyapatite monoliths formed by a dissolution-precipitation reaction at 38 °C can develop a tensile strength as high as 18 MPa. The compressive strength averages 174 MPa. Young's modulus is on the order of 6 GPa.

Increasing the liquid-to-solids ratio from 0.11 to 0.2 appears to increase internal flaws or microporosity more than surface flaws.

The compressive strength showed a variation with composition; calcium-deficient hydroxyapatite failed in tension while carbonated hydroxyapatite failed in shear. These variations appear to be related to compositionally dependent variations in morphology. The porosity in calcium-deficient hydroxyapatite appears to be uniformly distributed, occurring between grains which are interlocked by fibrous material. The porosity in the carbonated hydroxyapatite is far coarser than that in the calcium deficient material. Comparison of the two compositions suggests that improved mechanical properties are realized by a uniform distribution of fine porosity. A uniform pore structure in the calcium-deficient hydroxyapatite was observed microscopically. This is consistent with the

development of compressive properties comparable to those obtained in sintered hydroxyapatites having an equivalent total porosity. Thus, hydroxyapatite exhibiting compressive strengths comparable to those of sintered materials can be produced at physiological temperature.

Acknowledgement

The authors gratefully acknowledge the support of the National Institute of Dental Research, Grant R01-DE094-21-0184.

References

1. M. JARCHO, C. H. BOLEN, M. B. THOMAS, J. BOBICK, J. F. KAY and R. H. DOREMUS, *J. Mater. Sci.* **11** (1976) 2027.
2. F. A. PEYTON, *Ann. N.Y. Acad. Sci.* **146** (1968) 96.
3. R. L. BOWEN and M. S. RODRIGUEZ, *J. Amer. Dent. Assoc.* **64** (1962) 378.
4. N. E. WATERS, in *The mechanical properties of biological materials*, Symp. Soc. Exp. Biol. **34** (1980) 99.
5. G. de WITH, H. J. A. van DIJK, N. HATTU and K. PRIJS, *J. Mater. Sci.* **16** (1981) 1592.
6. D. WILLIAMS (ed.), in "Concise encyclopedia of medical and dental materials" (Pergamon, Oxford, 1990).
7. R. HASSAN, A. A. CAPUTO and R. F. BUNSHAH, *J. Dent. Res.* **60** (1981) 820.
8. M. AKAO, H. AOKI and K. KATO, *Rept. Inst. Med. Dent. Engr.* **15** (1981) 17.
9. H. AOKI, in "Science and medical applications of hydroxyapatite" (Takayama Press System Center Co., 1991).
10. W. E. BROWN and L. C. CHOW, in "Cements research progress – 1986", edited by P. W. Brown (American Ceramic Society, Westerville OH, 1987).
11. M. T. FULMER, R. I. MARTIN and P. W. BROWN, *J. Mater. Sci. Mater. Med.* **3** (1992) 299.
12. L. C. CHOW, S. TAKAGI, P. D. CONSTANTINO and C. D. FRIEDMAN, *Mater. Res. Soc. Proc.* **179** (1991) 3.
13. Y. FUKUSE, E. D. EANES, S. TAKAGI, L. C. CHOW and W. E. BROWN, *J. Dent. Res.* **69** (1990) 1852.
14. Y. TAKEZAWA, Y. DOI, S. SHIBATA, N. WAKAMATSU, T. GOTO, M. IIJIMA, Y. MORIWAKI, K. UNO, F. KUBO and Y. HAEUCHI, *Japan Soc. Dent. Mater. Devices* **7** (1988) 176.
15. R. I. MARTIN and BROWN, *J. Mater. Sci. Mater. Med.* in press.
16. A. RUDNICK, A. R. HUNER and F. C. HOLDEN, *Mater. Res. Standards* **3** (1963) 283.
17. F. P. BEER and E. R. JOHNSTON, Jr., in "Mechanics of materials" (McGraw-Hill, 1981).

Received 12 July 1993
and accepted 7 February 1994